

# The Quark-Photon Vertex and the Pion Charge Radius

Pieter Maris and Peter C. Tandy  
*Center for Nuclear Research, Department of Physics,  
Kent State University, Kent OH 44242*  
(October 12, 2018)

## Abstract

The rainbow truncation of the quark Dyson–Schwinger equation is combined with the ladder Bethe–Salpeter equation for the dressed quark-photon vertex to study the low-momentum behavior of the pion electromagnetic form factor. With model gluon parameters previously fixed by the pion mass and decay constant, the pion charge radius  $r_\pi$  is found to be in excellent agreement with the data. When the often-used Ball–Chiu Ansatz is used to construct the quark-photon vertex directly from the quark propagator, less than half of  $r_\pi^2$  is generated. The remainder of  $r_\pi^2$  is seen to be attributable to the presence of the  $\rho$ -pole in the solution of the ladder Bethe–Salpeter equation.

Pacs Numbers: 14.40.Aq, 13.40.Gp, 24.85.+p, 11.10.St, 12.38.Lg

## I. INTRODUCTION

For timelike photon momenta  $Q^2$  in the vicinity of the  $\rho$ -meson mass-shell, the pion charge form factor  $F_\pi(Q^2)$  will exhibit a resonant peak associated with the propagation of intermediate state  $\rho$ -mesons (we ignore a possible small effect due to  $\rho - \omega$  mixing). That is

$$F_\pi(Q^2) \rightarrow \frac{g_{\rho\pi\pi} m_\rho^2}{g_\rho (Q^2 + m_\rho^2 - im_\rho \Gamma_\rho)}, \quad (1)$$

in the Euclidean metric ( $Q^2 < 0$  corresponds to the timelike region) that we use throughout this work. Here  $m_\rho^2/g_\rho$  is the  $\rho - \gamma$  coupling strength fixed by the  $\rho \rightarrow e^+ e^-$  decay,  $g_{\rho\pi\pi}$  is the coupling constant for the  $\rho \rightarrow \pi\pi$  decay, and  $\Gamma_\rho$  is the  $\rho$  width which is principally due to the latter process. A long-standing issue in hadronic physics is the question of the extent to which  $F_\pi(Q^2)$  at low spacelike  $Q^2$  can be described by the  $\rho$ -resonance mechanism. This is an essential element of the vector meson dominance (VMD) model which is one of the earliest field theory models to be successful in a point coupling description of aspects of hadron dynamics. In the form of VMD where  $\rho - \gamma$  coupling is described by the contraction of the two field strength tensors  $\rho^{\mu\nu} F_{\mu\nu}$ , the pion charge form factor is produced as

$$F_\pi(Q^2) \approx 1 - \frac{g_{\rho\pi\pi} Q^2}{g_\rho (Q^2 + m_\rho^2 - im_\rho \Gamma_\rho(Q^2))}. \quad (2)$$

The non-resonant first term arises from the photon coupling to the charge of a point pion. The resonant second term arises from  $\rho - \gamma$  coupling, implements all of the  $Q^2$ -dependence, and vanishes at  $Q^2 = 0$  in accord with gauge invariance. The width  $\Gamma_\rho$  is nonzero beyond the threshold for  $\pi\pi$  production only, and the form factor is real for  $Q^2 > -4m_\pi^2$ . In this model the charge radius  $r_\pi^2 = -6F'_\pi(0)$  comes entirely from the resonant term and is  $6g_{\rho\pi\pi}/(m_\rho^2 g_\rho) = 0.48 \text{ fm}^2$ , which compares favorably with the experimental value  $0.44 \text{ fm}^2$ . See Ref. [1] for a recent review of the pion charge form factor and VMD in this form.

In terms of QCD, where the pion is a  $\bar{q}q$  bound state, the content of Eq. (2) cannot provide a realistic picture for  $F_\pi(Q^2)$  at (low) spacelike  $Q^2$ . The photon couples only to the distributed quark currents in the pion, the vector meson bound state is not a well-defined concept away from the pole, and the question of a resonant  $\rho$  contribution has to be addressed within the dressed quark-photon vertex. This is the topic we explore in this work. Given that one can find a convenient (and necessarily model-dependent) representation of the quark-photon vertex involving direct and resonant parts, the direct coupling will necessarily produce a distribution  $F_\pi^{dir}(Q^2)$  to replace the first term in Eq. (2) and there will be a corresponding contribution to the charge radius. The remaining contribution must differ from the second term of Eq. (2) because  $g_{\rho\pi\pi}$ ,  $g_\rho$ ,  $m_\rho$  and  $\Gamma_\rho$  are well-defined only for the physical on-shell vector meson bound state. A measure of the ambiguities involved is provided by a recent study that modeled the underlying  $\bar{q}q$  substructure of  $\rho$  and  $\pi$ . Under the assumption that the  $\rho$  Bethe-Salpeter (BS) amplitude is applicable also at  $Q^2 = 0$ , it was found that  $g_{\rho\pi\pi}^{\text{eff}}(Q^2 = 0) \approx g_{\rho\pi\pi}/2$  [2]. On face value, this suggests that only about 50% of  $r_\pi^2$  would be attributable to the  $\rho$ -resonance mechanism.

In this work we obtain the quark-photon vertex as the solution of the inhomogeneous Bethe-Salpeter equation (BSE) in ladder truncation with the dressed quark propagators

taken as solutions of the Dyson–Schwinger equation (DSE) in rainbow truncation. Such a procedure automatically incorporates the pole structure of the vertex corresponding to the vector meson spectrum of the homogeneous BSE. A previous exploratory study [3] of the coupled DSE–BSE for the quark propagator and the quark-photon vertex employed a simple infrared dominant form of the effective gluon propagator in order to utilize closed form expressions for the dressed quark propagators and the resulting BSE kernel. That study was not carried far enough to draw implications for the pion form factor.

We employ a more realistic model for the effective quark-antiquark coupling that has recently been shown to reproduce the pion and kaon masses and decay constants [4] as well as the masses and decay constants for the vector mesons  $\rho$ ,  $\phi$  and  $K^*$  to within 10% [5]. There, as well as here, the quark propagators are consistently dressed through the quark DSE using the same effective gluon propagator, which ensures that the vector Ward–Takahashi identity is obeyed and electromagnetic current is conserved. The model parameters are all fixed in previous work [5] and constrained only by  $m_\pi$ ,  $m_K$ ,  $f_\pi$  and  $\langle \bar{q}q \rangle$ .

Next, we use this quark-photon vertex to investigate the low momentum behavior of the pion charge form factor. The results are compared to those from the Ball–Chiu (BC) Ansatz for the vertex which is commonly used in such studies. In comparison with the results from the BSE solution, use of the BC Ansatz (and variations thereof) underestimates the charge radius. The BC Ansatz does not have the vector meson pole that is naturally present within the BSE solution. We explore the extent to which the BSE solution for the vertex can be reproduced by the addition of a suitable  $\rho$ -pole term to the BC Ansatz. We then assess the performance of this “resonant-improved” Ansatz for the quark-photon vertex.

In Sec. II we review the formulation that underlies recent studies of the pion form factor within a modeling of QCD through the DSEs, and discuss the need for a dressed quark-photon vertex in such models. The BSE for the quark-photon vertex is described in Sec. III and the vector meson pole contributions are outlined. Also described there are: the model used for the effective coupling in ladder truncation, the basis of covariants used, and the comparison of the numerical solution with the resonant-improved BC Ansatz. Our analysis of the low-momentum behavior of the pion form factor and charge radius is presented in Sec. IV, and concluding remarks are given in Sec. V.

## II. THE PION ELECTROMAGNETIC FORM FACTOR

A number of works have treated the electromagnetic form factors of pions [6,7], kaons [8,9], and more recently vector mesons [10] and nucleons [11] in the course of QCD modeling via truncations of the DSEs. Using dressed quark propagators and bound state BS amplitudes, form factors can be calculated in impulse approximation, as depicted in Fig. 1 for the  $\gamma\pi\pi$  vertex. Such work proceeds most easily in Euclidean metric  $\{\gamma_\mu, \gamma_\nu\} = 2\delta_{\mu\nu}$ ,  $\gamma_\mu^\dagger = \gamma_\mu$  and  $a \cdot b = \sum_{i=1}^4 a_i b_i$ . In the space of color, flavor and Dirac spin, we denote by  $\tilde{\Gamma}_\mu(p; Q)$  the quark-photon vertex describing the coupling of a photon with momentum  $Q$  to a quark with initial and final momenta  $p - Q/2$  and  $p + Q/2$  respectively. With this notation, the  $\gamma\pi\pi$  vertex takes the form

$$\Lambda_\nu(P, Q) = 2P_\nu F_\pi(Q^2)$$

$$= -2 \int \frac{d^4q}{(2\pi)^4} \text{Tr} \left[ \Gamma_\pi(k_+; -P_+) S(q_{+-}) i\tilde{\Gamma}_\nu(q_+; Q) S(q_{++}) \Gamma_\pi(k_-; P_-) S(q_-) \right], \quad (3)$$

where  $F_\pi(Q^2)$  is the pion form factor and  $P_\pm = P \pm Q/2$ ,  $q_\pm = q \pm P/2$ ,  $q_{\pm\pm} = q_\pm \pm Q/2$  and  $k_\pm = q \pm Q/4$ .  $S(q)$  is the dressed quark propagator,  $\Gamma_\pi(k; P)$  is the pion BS amplitude corresponding to relative  $\bar{q}q$  momentum  $k$  (we choose equal partitioning) and pion momentum  $P$ , and  $\text{Tr}[\dots]$  denotes the trace over color, flavor and spin indices. The quark-photon vertex  $\tilde{\Gamma}_\nu(q; Q)$  at sufficiently large spacelike  $Q^2$  becomes  $\tilde{\Gamma}_\nu(q; Q) \rightarrow \hat{Q} \gamma_\mu$ , where  $\hat{Q}$  is the quark charge operator.

The quark-photon vertex satisfies the Ward–Takahashi identity (WTI)

$$i Q_\mu \tilde{\Gamma}_\mu(p; Q) = \hat{Q} (S^{-1}(p + Q/2) - S^{-1}(p - Q/2)), \quad (4)$$

as a result of gauge invariance. At  $Q = 0$  the vertex is completely specified by the differential Ward identity

$$i \tilde{\Gamma}_\mu(p; 0) = \hat{Q} \frac{\partial}{\partial p_\mu} S(p)^{-1}. \quad (5)$$

This reduces Eq. (3) to  $F_\pi(Q^2 = 0) = 1$  if  $\Gamma_\pi$  is properly normalized<sup>1</sup>. This clearly shows that the bare vertex  $\gamma_\mu$  is generally a bad approximation due to the momentum-dependence of the quark self-energy: only with bare quark propagators, does a bare vertex satisfy Eqs. (4) and (5). Use of a bare vertex, in combination with dressed propagators, in Eq. (3), violates charge conservation and leads to  $F_\pi(0) \neq 1$ .

The WTI determines the longitudinal part of the vertex completely in terms of the (inverse) quark propagator. However, the transverse part is largely unconstrained by symmetries. A common Ansatz for the dressed vertex is that due to Ball and Chiu [12] which was developed in the context of QED investigations and is a representation in terms of the quark propagator functions  $A$  and  $B$  defined by

$$S(p)^{-1} = i \not{p} A(p^2) + B(p^2). \quad (6)$$

With  $\tilde{\Gamma}_\mu^{\text{BC}}(p; Q) = \hat{Q} \Gamma_\mu^{\text{BC}}(p; Q)$  the BC Ansatz is

$$\Gamma_\mu^{\text{BC}}(p; Q) = \frac{1}{2} \gamma_\mu \left( A(p_+) + A(p_-) \right) + 2 \not{p} p_\mu \frac{A(p_+) - A(p_-)}{p_+^2 - p_-^2} - 2 i p_\mu \frac{B(p_+) - B(p_-)}{p_+^2 - p_-^2}, \quad (7)$$

where  $p_\pm = p \pm Q/2$ . This satisfies the constraints from the WTI Eq. (4) and the Ward identity Eq. (5), transforms under CPT as a vector vertex should, and has the correct perturbative limit  $\gamma_\mu$  in the ultraviolet. The longitudinal part of  $\Gamma_\mu^{\text{BC}}$  is exact; the transverse part is exact only at  $Q = 0$  and in the UV limit. Curtis and Pennington have explored the additional Dirac structures that are possible for the transverse part of the vertex and have suggested an improved Ansatz [13] based on multiplicative renormalizability in QED

---

<sup>1</sup>This equivalence holds if the kernel of the pion BSE is independent of the pion momentum. For the ladder truncation of the kernel, which we consider here, this is the case.

$$\Gamma_{\mu}^{\text{CP}}(p; Q) = \Gamma_{\mu}^{\text{BC}}(p; Q) + \left( (p_+^2 - p_-^2) \gamma_{\mu} - (\not{p}_+ - \not{p}_-) p_{\mu} \right) \frac{(p_+^2 + p_-^2)(A(p_+) - A(p_-))}{(p_+^2 - p_-^2)^2 + (M(p_+)^2 + M(p_-)^2)^2}, \quad (8)$$

with  $M(p) = B(p)/A(p)$ . Both Ansätze Eq. (7) and Eq. (8) for the  $\bar{q}q\gamma$  vertex satisfy all symmetry constraints, and use of them in Eq. (3) leads to  $F_{\pi}(0) = 1$ , but neither of them contain the timelike vector meson poles of the exact vertex.

The pion charge radius

$$r_{\pi}^2 = -6 \left. \frac{\partial F_{\pi}(Q^2)}{\partial Q^2} \right|_{Q^2=0}, \quad (9)$$

will receive two types of contribution within the impulse approximation in Eq. (3): 1) contributions from  $\tilde{\Gamma}_{\nu}(Q=0)$  coupled with the  $Q^2$ -slope produced by the quark propagators and  $\Gamma_{\pi}$ , and 2) contributions proportional to the  $Q^2$ -slope of  $\tilde{\Gamma}_{\nu}(Q)$ . For the first type, use of the BC Ansatz is sufficient since the BC Ansatz is exact at  $Q=0$ . However for the second type of contribution,  $\partial\tilde{\Gamma}_{\mu}(p; Q)/\partial Q^2$  is *not* constrained by symmetries.

Previous studies of three-point quark loops such as Eq. (3) for form factors have, for practical reasons, utilized parameterized representations of the DSE solutions for quark propagators and the BS amplitudes, in conjunction with the BC Ansatz for the quark-photon vertex [6–10]. The parameters are fitted to give a good description of pion and related chiral observables such as  $f_{\pi}$ ,  $m_{\pi}$ ,  $r_{\pi}$ , and  $\langle\bar{q}q\rangle$  with a view towards parameter-free studies of other mesons and observables [14]. This procedure can produce values of  $r_{\pi}^2$  in the range 20% to 30% below the experimental value [7,14], which leaves some room for additional contributions, such as those coming from  $\pi\pi$  rescattering [15] and from the  $\rho$ -resonance mechanism. However the estimated 50% of  $r_{\pi}^2$  being due to the  $\rho$ -resonance [2] appears to be incompatible with these parametrizations.

Here, we reconcile the VMD picture with the QCD picture of a photon coupled to distributed quarks in a  $\bar{q}q$  bound state by calculating all ingredients needed for  $F_{\pi}(Q^2)$  via Eq. (3) from their dynamical equations: we solve the quark DSE, the pion BSE, and the inhomogeneous vertex BSE in a self-consistent way, using the same model for the effective quark-antiquark coupling. Both resonance and non-resonance contributions to the vertex are dynamically generated through the BSE. By comparison with the BC Ansatz we can identify resonance contributions; however, one must keep in mind that such an identification is necessarily model-dependent.

### III. THE BETHE–SALPETER SOLUTION FOR THE VECTOR VERTEX

The quark-photon vertex satisfies the renormalized inhomogeneous BSE

$$\tilde{\Gamma}_{\mu}(p; Q) = Z_2 \hat{Q} \gamma_{\mu} + \int^{\Lambda} \frac{d^4q}{(2\pi)^4} K(p, q; Q) S(q + \eta Q) \tilde{\Gamma}_{\mu}(q; Q) S(q - \bar{\eta} Q), \quad (10)$$

where  $\eta + \bar{\eta} = 1$  describes the momentum sharing between the two quarks. The kernel  $K$  operates in the direct product space of color, flavor and Dirac spin for the quark and antiquark and is the renormalized, amputated  $\bar{q}q$  scattering kernel that is irreducible with

respect to a pair of  $\bar{q}q$  lines. The notation  $\int^\Lambda$  denotes a translationally-invariant regularization of the integral, with  $\Lambda$  the regularization mass-scale. At the end of all calculations the regularization is removed by taking the limit  $\Lambda \rightarrow \infty$ .

The renormalization constant  $Z_2$  and the renormalized dressed quark propagator  $S$  follow from the quark DSE

$$S(p)^{-1} = Z_2 i \not{p} + Z_4 m(\mu) + Z_1 \int^\Lambda \frac{d^4 q}{(2\pi)^4} g^2 D_{\mu\nu}(p-q) \frac{\lambda^a}{2} \gamma_\mu S(q) \Gamma_\nu^a(q, p), \quad (11)$$

where  $D_{\mu\nu}(k)$  is the renormalized dressed-gluon propagator and  $\Gamma_\nu^a(q; p)$  is the renormalized dressed-quark-gluon vertex. The solution of Eq. (11) is renormalized according to

$$S(p)^{-1} \Big|_{p^2=\mu^2} = i \not{p} + m(\mu), \quad (12)$$

at a sufficiently large spacelike  $\mu^2$ , with  $m(\mu)$  the renormalized quark mass at the scale  $\mu$ . In Eq. (11),  $S$ ,  $\Gamma_\mu^a$  and  $m(\mu)$  depend on the quark flavor, although we have not indicated this explicitly. The renormalization constants depend on the renormalization point and the regularization mass-scale, but not on flavor: in our analysis we employ a flavor-independent renormalization scheme.

### A. Bound state contributions

Solutions of the homogeneous version of Eq. (10) at discrete timelike momenta  $Q^2$  define vector meson bound states with masses  $m_n^2 = -Q^2$ . It follows that  $\tilde{\Gamma}_\mu(p; Q)$  has poles at those locations. The corresponding resonant form can be obtained by observing that Eq. (10) has the equivalent form

$$\tilde{\Gamma}_\mu(p; Q) = Z_2 \hat{Q} \gamma_\mu + Z_2 \int^\Lambda \frac{d^4 q}{(2\pi)^4} M(p, q; Q) S(q + \eta Q) \hat{Q} \gamma_\mu S(q - \bar{\eta} Q), \quad (13)$$

with  $M$  being the  $\bar{q}q$  scattering amplitude given in schematic form by  $M = K + K S M S$ . In the vicinity of the timelike points  $Q^2 = -m_n^2$  where the homogeneous BSE has solutions,  $M$  has poles with residues that define the physical meson BS amplitudes. In particular, for two flavors,

$$M(p, q; Q) \rightarrow -\frac{\Gamma_\nu^\rho(p; Q) \bar{\Gamma}_\nu^\rho(q; -Q)}{Q^2 + m_\rho^2} - \frac{\Gamma_\nu^\omega(p; Q) \bar{\Gamma}_\nu^\omega(q; -Q)}{Q^2 + m_\omega^2}, \quad (14)$$

with the BS amplitudes properly normalized. In the ladder truncation that we will be concerned with in practice, the normalization condition reduces to ( $n = \rho^0, \omega$ )

$$2P_\mu = \frac{\partial}{\partial P_\mu} \frac{1}{3} \int^\Lambda \frac{d^4 q}{(2\pi)^4} \text{Tr} \left[ \bar{\Gamma}_\nu^n(q; -K) S(q + \eta P) \Gamma_\nu^n(q; K) S(q - \bar{\eta} P) \right] \Big|_{P^2=K^2=-m^2}, \quad (15)$$

where the factor  $1/3$  appears because the three transverse directions are summed. Using the fact that massive vector mesons are transverse, the resonant form of the quark-photon vertex near the vector meson poles can be written as

$$\tilde{\Gamma}_\mu(p; Q) \rightarrow \frac{\Gamma_\mu^\rho(p; Q)m_\rho^2/g_\rho}{Q^2 + M_\rho^2} + \frac{\Gamma_\mu^\omega(p; Q)m_\omega^2/g_\omega}{Q^2 + M_\omega^2}, \quad (16)$$

where the coupling constants  $g_n$  ( $n = \rho^0, \omega$ ) for  $\rho - \gamma$  and  $\omega - \gamma$  mixing are

$$\frac{m_n^2}{g_n} = -\frac{Z_2}{3} \int^\Lambda \frac{d^4q}{(2\pi)^4} \text{Tr} \left[ \bar{\Gamma}_\nu^n(q; -Q) S(q + \eta Q) \hat{Q} \gamma_\nu S(q - \bar{\eta} Q) \right]. \quad (17)$$

Away from the pole, the separation into a resonant and non-resonant part is not unique; the solution of the BSE for the complete vertex contains both aspects in a consistent way.

At the level of the ladder approximation, which is commonly used in practical calculations, and using isospin symmetry, we have  $m_\rho = m_\omega = m_V$ , and the flavor structure of the BS amplitudes is  $\Gamma_\nu^\rho(p; Q) = (\tau_3/\sqrt{2})\Gamma_\nu^V(p; Q)$ , and  $\Gamma_\nu^\omega(p; Q) = (1/\sqrt{2})\Gamma_\nu^V(p; Q)$ . The flavor trace in Eq. (17) gives  $g_\omega = 3g_\rho = 3g_V$ . The factorization  $\tilde{\Gamma}_\mu = \hat{Q}\Gamma_\mu$  allows Eq. (16) for the vector pole structure to simplify to the flavor-independent form

$$\Gamma_\mu(p; Q) \rightarrow \frac{\Gamma_\mu^V(p; Q)f_V m_V}{Q^2 + m_V^2}, \quad (18)$$

where  $f_V m_V = \sqrt{2}m_V^2/g_V$ . Our numerical study is carried out for the flavor-independent vector vertex  $\Gamma_\mu(p; Q)$ .

## B. Ladder–rainbow truncation

We use a ladder truncation for the BSE

$$K_{tu}^{rs}(p, q; P) \rightarrow -\mathcal{G}((p - q)^2) D_{\mu\nu}^{\text{free}}(p - q) \left( \frac{\lambda^a}{2} \gamma_\mu \right)^{ru} \otimes \left( \frac{\lambda^a}{2} \gamma_\nu \right)^{ts}, \quad (19)$$

where  $D_{\mu\nu}^{\text{free}}(k)$  is the perturbative gluon propagator in Landau gauge. The resulting BSE is consistent with a rainbow truncation  $\Gamma_\nu^a(q, p) \rightarrow \gamma_\nu \lambda^a/2$  for the quark DSE, Eq. (11), in the sense that the combination produces vector and axial-vector vertices satisfying the respective WTIs. In the axial case, this ensures that in the chiral limit the ground state pseudoscalar mesons are massless even though the quark mass functions are strongly enhanced in the infrared [4,16]. In the vector case, this ensures electromagnetic current conservation.

The model is completely specified once a form is chosen for the “effective coupling”  $\mathcal{G}(k^2)$ . We employ the Ansatz [4,5]

$$\frac{\mathcal{G}(k^2)}{k^2} = \frac{4\pi^2}{\omega^6} D k^2 e^{-k^2/\omega^2} + 4\pi \frac{\gamma_m \pi}{\frac{1}{2} \ln \left[ \tau + (1 + k^2/\Lambda_{\text{QCD}}^2)^2 \right]} \mathcal{F}(k^2), \quad (20)$$

with  $\mathcal{F}(k^2) = [1 - \exp(-k^2/[4m_t^2])]/k^2$ , and  $\gamma_m = 12/(33 - 2N_f)$ . This Ansatz preserves the one-loop renormalization group behavior of QCD for solutions of the quark DSE. In particular, it produces the correct one-loop QCD anomalous dimension of the quark mass function  $M(p^2)$  for both the chiral limit and explicit chirally broken case [4,17]. The first term of Eq. (20) implements the strong infrared enhancement in the region  $k^2 = 0 - 1 \text{ GeV}^2$

which is a phenomenological requirement for sufficient dynamical chiral symmetry breaking to produce an acceptable strength for the quark condensate [18]. We use  $m_t = 0.5$  GeV,  $\tau = e^2 - 1$ ,  $N_f = 4$ ,  $\Lambda_{\text{QCD}}^{N_f=4} = 0.234$  GeV, and a renormalization point  $\mu = 19$  GeV, which is sufficiently perturbative to allow the one-loop asymptotic behavior of the quark propagator to be used as a check [4,5]. The remaining parameters are fixed to  $\omega = 0.4$  GeV and  $D = 0.93$  GeV<sup>2</sup> to give a good description of  $m_{\pi/K}$  and  $f_\pi$ . The subsequent values for  $f_K$  and the masses and decay constants of the vector mesons  $\rho, \phi, K^*$  are very well described [5].

### C. Numerical solution

The general form of  $\Gamma_\mu(q; Q)$  can be decomposed into twelve independent Lorentz covariants, made from the three vectors  $\gamma_\mu$ , the relative momentum  $q_\mu$ , and the photon momentum  $Q_\mu$ , each multiplied by one of the four independent matrices  $\mathbb{1}$ ,  $\not{q}$ ,  $\not{Q}$ , and  $\sigma_{\mu\nu}q_\mu Q_\nu$ . Four of the covariants represent the longitudinal components which are completely specified by the WTI and can be taken as the longitudinal projection  $\Gamma_\mu^L$  of the BC Ansatz, Eq. (7). The solution of the BSE for the transverse vertex can be expanded in eight covariants  $T_\mu^i(q; Q)$ . Thus the total vertex is decomposed as

$$\Gamma_\mu(q; Q) = \Gamma_\mu^L(q; Q) + \sum_{i=1}^8 T_\mu^i(q; Q) F_i(q^2, q \cdot Q; Q^2), \quad (21)$$

with the invariant amplitudes  $F_i$  being Lorentz scalar functions. The choice for the covariants  $T_\mu^i(q; Q)$  to be used as a basis is constrained by the required properties under Lorentz and CPT transformations, but is not unique. The BSE, Eq. (10), must be projected onto the covariant basis to produce a coupled set of eight linear equations for the invariant amplitudes  $F_i$  to be cast in matrix form. This requires a procedure to project out a single amplitude from the general form Eq. (21). It is therefore helpful if the chosen covariants satisfy a Dirac-trace orthogonality property. The following set of orthogonal covariants is used here<sup>2</sup>

$$T_\mu^1(q; Q) = \gamma_\mu^T, \quad (22)$$

$$T_\mu^2(q; Q) = (q_\mu^T \not{q}^T - \frac{1}{3} \gamma_\mu^T (q^T)^2) / q^2, \quad (23)$$

$$T_\mu^3(q; Q) = q_\mu^T \not{Q} q \cdot Q / (q^2 Q^2), \quad (24)$$

$$T_\mu^4(q; Q) = -(\gamma_\mu^T [\not{Q}, \not{q}] + 2 q_\mu^T \not{Q}) / 2q, \quad (25)$$

$$T_\mu^5(q; Q) = i q_\mu^T / q, \quad (26)$$

$$T_\mu^6(q; Q) = i [\gamma_\mu^T, \not{q}^T] q \cdot Q / q^2, \quad (27)$$

$$T_\mu^7(q; Q) = i [\gamma_\mu^T, \not{Q}] (1 - \cos^2 \theta) - 2 T_\mu^8(q; Q), \quad (28)$$

$$T_\mu^8(q; Q) = i q_\mu^T \not{q}^T \not{Q} / q^2, \quad (29)$$

---

<sup>2</sup>Since the domain of interest here includes both timelike and spacelike  $Q^2$ , we avoid factors of  $Q = \sqrt{Q^2}$ . Therefore we do not require the covariants to be normalized, as we did in Ref. [5]. We also include explicit factors of  $q \cdot Q$  in  $T_3$  and  $T_6$  so that now every  $F_i$  is even in  $q \cdot Q$ .



where  $V^T$  is the component of  $V$  transverse to  $Q$ , that is  $V_\mu^T = V_\mu - Q_\mu(Q \cdot V)/Q^2$  and  $q \cdot Q = qQ \cos \theta$ . Each amplitude can be projected onto a basis of even-order Chebyshev polynomials in  $\cos \theta$  to produce  ${}^n F_i(q^2, Q^2)$  [5]. It is found that terms beyond the zeroth order,  $n > 0$ , are insignificant and are not used in the subsequent study of the form factor.

For a range of small timelike and spacelike  $Q^2$ , the ratio of the BSE solution to the BC Ansatz for the dominant amplitude  ${}^0 F_1$  is displayed in Fig. 2 as function of  $q^2$ . The deviation from unity indicates differences between the BC Ansatz and our numerical solution of the ladder BSE. It is immediately obvious that for timelike photon momenta and  $q^2 < 3 \text{ GeV}^2$  there is a significant enhancement of the BSE solution compared to the BC Ansatz. This strong increase in the vertex BSE solution is due to the vector meson pole at  $Q^2 \approx -0.55 \text{ GeV}^2$ , which only affects the vertex at small  $q^2$ ; at large  $q^2$  both the BSE solution and the BC Ansatz approach the bare vertex for any value of  $Q^2$ .

Charge conservation is evident through the ratio being one at  $Q = 0$ : the ladder vertex BSE solution satisfies the WTI. The fact that our numerical solution indeed is to within 1% equal to the BC Ansatz, not only for  ${}^0 F_1$ , but also for the other amplitudes, indicates the accuracy of our numerical methods. At small spacelike momenta the BSE solution differs considerably from the BC Ansatz. The difference increases with  $Q^2$  in the range  $0 < Q^2 < 2 \text{ GeV}^2$ ; it is only at asymptotic values of  $Q^2$  that they become equal again.

A different perspective is shown by Fig. 3 which compares the  $Q^2$ -dependence of  ${}^0 F_1$  at  $q^2 = 0$ . Again, the agreement at  $Q^2 = 0$  is dictated by the Ward identity; however, the slope of  ${}^0 F_1(0, Q^2)$  at  $Q^2 = 0$  as obtained from the vertex BSE solution differs significantly from that produced by the BC Ansatz. This can be of importance for the charge radii of the pion and other hadrons. In this figure one can clearly see the presence of the vector pole in the  $\bar{q}q\gamma$  vertex at  $Q^2 \approx -0.55 \text{ GeV}^2$ . Also in this figure we plot the amplitude  ${}^0 F_1$  as obtained from the BC Ansatz with the quark propagators of Ref. [7], which were parameterized rather than obtained as the solution of a DSE. The parameters were fitted to  $f_\pi$ ,  $m_\pi$ ,  $r_\pi$ , and  $\langle \bar{q}q \rangle$ , using the BC Ansatz in the calculation of  $r_\pi$ . The  $Q^2$ -dependence of the  $\bar{q}q\gamma$  vertex necessary in order to reproduce a reasonable value for  $r_\pi$  was thus incorporated via the quark propagator functions. We see that this phenomenological vertex amplitude has indeed a much stronger  $Q^2$ -dependence than is obtained by use of the present DSE solution for the quark propagator in the BC Ansatz. This phenomenological procedure allows one to get reasonable electromagnetic form factors at low  $Q^2$  without explicitly taking resonances into account.

We have investigated the extent to which the vertex BSE solution can be represented by the interpolating form

$$\Gamma_\mu(q; Q) \simeq \Gamma_\mu^{\text{BC}}(q; Q) - \sum_i T_\mu^i(q; Q) F_i^V(q^2) \frac{f_V Q^2}{m_V(Q^2 + m_V^2)}, \quad (30)$$

where  $F_i^V$  are the leading Chebyshev moments of the mass-shell vector meson BS amplitudes produced by the present model [5]. The second term Eq. (30) correctly describes the vertex near the vector meson pole at  $Q^2 = -m_V^2$ ; there is no width generated for the vector meson in the present ladder truncation of the BSE. One would have to add the  $\pi\pi$  channel to the ladder BSE kernel to produce a  $\rho$  width; for the vertex, this would generate an imaginary part beyond the threshold for pion production,  $Q^2 < -4m_\pi^2$ .

For small spacelike  $Q^2$ , Eq. (30) represents an extrapolation consistent with: a)  $\Gamma^{\text{BC}}(q; Q = 0)$  is exact due to gauge invariance and b) the  $\rho - \gamma$  coupling should not generate a photon mass. Over the limited domain  $-m_V^2 < Q^2 < 0.2 \text{ GeV}^2$ , Eq. (30) produces a very good representation of the vertex amplitudes  ${}^0F_1$ ,  ${}^0F_3$  and  ${}^0F_5$  and a quite reasonable representation for the remainder, except for  ${}^0F_4$  which is clearly the worst case, and the hardest to represent in a resonance formula. In Figs. 4, 5 and 6, this approximate form is compared to the vertex BSE solution for the three dominant amplitudes  ${}^0F_1$ ,  ${}^0F_4$  and  ${}^0F_5$ .

In this sense we shall refer to the BC Ansatz as missing a contribution near the  $\rho$  pole, and to Eq. (30) as a resonant-improved BC Ansatz applicable in the region  $-0.4 \text{ GeV}^2 < Q^2 < 0.2 \text{ GeV}^2$  only. At asymptotic  $Q^2$ , this form is obviously not adequate: it does not go to the bare vertex. Close to the  $\rho$  pole, neither our vertex BSE solution nor the interpolating form Eq. (30) are physically realistic, because neither one takes into account the width  $\Gamma_\rho$  generated by the open  $\pi\pi$  decay channel. Since  $\Gamma_\rho/m_\rho \sim 0.2$ , the width contributes little for  $Q^2 > -0.4 \text{ GeV}^2$ , and the  $\rho$  contribution can be approximated by the simple pole term in Eq. (30) for applications such as the pion form factor calculation.

#### IV. RESULTS FOR THE PION FORM FACTOR

In addition to the solution of the BSE for the  $\bar{q}q\gamma$  vertex and the quark propagator  $S$  as the solution of its DSE, we also need the pion BS amplitude  $\Gamma_\pi(q; P)$ . This BS amplitude is the solution of a homogeneous BSE, and for pseudoscalar bound states it has the form [4]

$$\Gamma_\pi(q; P) = \gamma_5 [iE_\pi(q; P) + \not{P} F_\pi(q; P) + \not{q} q \cdot P G_\pi(q; P) + \sigma_{\mu\nu} q_\mu P_\nu H_\pi(q; P)] , \quad (31)$$

with the invariant amplitudes  $E_\pi$ ,  $F_\pi$ ,  $G_\pi$  and  $H_\pi$  being Lorentz scalar functions of  $q^2$  and  $q \cdot P = qP \cos\theta$ , with  $P^2 = -m_\pi^2$  the fixed, on-shell, pion momentum. Each amplitude can be projected onto a basis of even-order Chebyshev polynomials in  $\cos\theta$  and in Ref. [4] it was found that terms beyond the zeroth order are insignificant. With these ingredients we can now calculate the pion electromagnetic form factor in impulse approximation, Eq. (3).

In Fig. 7 we show our results for the pion form factor for a range of timelike and spacelike  $Q^2$  using the BSE solution for the  $\bar{q}q\gamma$  vertex, and compare our results with various other treatments of this vertex. Clearly a bare quark-photon vertex is incorrect: current conservation, which ensures  $F_\pi(0) = 1$ , is violated. Use of the BC Ansatz conserves the current because it satisfies the vector Ward identity. However the resulting form factor misses the data completely; the  $Q^2$ -dependence is clearly too small. On the other hand, the BSE solution for the vertex gives an excellent description of the low  $Q^2$  data, both in the spacelike and timelike region, *without fine tuning the model parameters*: the parameters are completely fixed by  $m_\pi$  and  $f_\pi$  in Ref. [5]. The use of the Curtis–Pennington Ansatz, Eq. (8), gives results for the form factor essentially the same as those obtained with the BC Ansatz.

Experimentally, the form factor shows a resonance peak at  $Q^2 = -m_\rho^2 = -0.593 \text{ GeV}^2$ . Our calculated  $F_\pi(Q^2)$  using the BSE solution diverges as  $1/(Q^2 + m_V^2)$  as one approaches  $Q^2 = -m_V^2 \approx -0.55 \text{ GeV}^2$ , where the homogeneous BSE admits a bound state solution: in the ladder truncation for the BSE one does not get a width for the  $\rho$  meson. We expect that if we incorporate the open decay channel  $\rho \rightarrow \pi\pi$  in the BSE kernel to generate a

width  $\Gamma_\rho$  for the  $\rho$ , we will have better agreement with the data close to the resonance peak. In addition, some of the present difference between our calculation and the data in the resonance region is due to the fact that our numerical value for  $m_\rho$  is about 4% below the physical  $\rho$  mass.

Four of the eight amplitudes,  $F_3$ ,  $F_6$ ,  $F_7$ , and  $F_8$ , contribute less than 1% to  $F_\pi(Q^2)$  on the  $Q^2$ -range considered. Although the amplitude  $F_3$  contributes very little to the form factor, this amplitude is needed for strict charge conservation. Therefore we can truncate the BSE solution to the dominant five covariants  $F_1$  through  $F_5$  without significantly changing the description of  $F_\pi(Q^2)$ . In Fig. 7, the result using the five dominant amplitudes is almost indistinguishable from the results obtained with all eight amplitudes.

The relative contributions to  $F_\pi(Q^2)$  from the amplitudes  $F_1$ ,  $F_2$ ,  $F_4$ , and  $F_5$  of the vertex BSE solution are displayed in Fig. 8. This shows that the canonical amplitude  $F_1$ , together with the canonical (pseudoscalar) amplitude  $E_\pi$  of the pion, generates the bulk of the form factor in the infrared region. The pion pseudovector amplitudes  $F_\pi$  and  $G_\pi$  give a negative contribution of about 25% near  $Q^2 = 0$ , but they are known to dominate at large  $Q^2$ : the asymptotic behavior of the form factor,  $F_\pi(Q^2) \sim 1/Q^2$ , is governed by the pseudovector amplitudes of the pion [7]. The vertex amplitudes  $F_2$ ,  $F_4$ , and  $F_5$  give negative contributions to  $F_\pi$  of the order of 10% at small  $Q^2$ . Of particular note is the contribution from amplitude  $F_4$ . Due to the Ward identity, this vertex contribution, and hence its contribution to  $F_\pi(Q^2)$ , must vanish at  $Q^2 = 0$ . The latter is indeed evident in Fig. 8; it is also evident there that this amplitude nevertheless is one of the important contributors to the slope and hence  $r_\pi$ ; its contribution to the form factor grows roughly linear with  $Q^2$  in the range we studied. This could have significant consequences for the form factor at intermediate energies. At asymptotic values of  $Q^2$  the  $\bar{q}q\gamma$  vertex approaches the bare vertex, and thus all functions  $F_i$  except for  $F_1$  will vanish. The asymptotic behavior of the form factor is therefore not influenced by  $F_4$  nor any other subdominant amplitude of the  $\bar{q}q\gamma$  vertex.

In terms of the pion charge radius  $r_\pi$ , these results are summarized in Table I. It is seen that, compared to the empirical value  $r_\pi^2 = 0.44 \text{ fm}^2$ , the BSE solution for the vertex generates an excellent value:  $r_\pi^2 = 0.46 \text{ fm}^2$  using all eight transverse covariants or using the dominant five,  $F_1$  through  $F_5$ . The BC Ansatz produces a value for  $r_\pi^2$  that is less than half this value; this is also evident in Fig. 7. The main reason for this is that the  $\bar{q}q\gamma$  vertex at small but non-zero  $Q^2$  is poorly represented by the BC Ansatz, as shown, for example, in Fig. 3. The Curtis–Pennington Ansatz gives almost the same charge radius as the BC Ansatz.

### A. Resonance contribution to $r_\pi$

In the previous section we found that the vertex BSE solution could be simulated by a resonant-improved BC Ansatz, Eq. (30). The use of such a form for the  $\bar{q}q\gamma$  vertex yields, via the impulse approximation Eq. (3), a charge form factor that can be expressed as

$$F_\pi(Q^2) \approx F_\pi^{\text{BC}}(Q^2) - \frac{g_{\rho\pi\pi} F_{V\pi\pi}(Q^2) Q^2}{g_\rho(Q^2 + m_\rho^2)}, \quad (32)$$

where  $F_\pi^{\text{BC}}(Q^2)$  is the result from the BC Ansatz. The combination  $g_{\rho\pi\pi} F_{V\pi\pi}$  represents the  $\pi\pi$  coupling to the vector  $\bar{q}q$  correlation  $T_\mu^i F_i^V$  evident in the resonant term of Eq. (30).

The behavior of this latter term guarantees that at the vector meson pole, the second term of Eq. (32) reproduces the standard behavior and  $F_{V\pi\pi}(-m_\rho^2) = 1$ . For other  $Q^2$  values  $F_{V\pi\pi}(Q^2)$  does not correspond to a physical process: off-shell mesons are by definition not physical. However, the departure of  $F_{V\pi\pi}(Q^2)$  from unity is a rough measure of the difference in  $\pi\pi$  coupling experienced by the effective vector  $\bar{q}q$  correlation away from the  $\rho$  mass-shell compared to the physical  $\rho\pi\pi$  coupling.

The charge form factor resulting from two versions of the resonant-improved BC Ansatz are shown in Fig. 9. One version is based on the five dominant invariant amplitudes  ${}^0F_i^V(q^2)$  of the  $\rho$  meson, the other uses only the single dominant amplitude  ${}^0F_1^V(q^2)$ ; physical normalization is imposed in each case. The employed values of  $m_\rho$  and  $f_\rho$  in each case are those obtained consistently from the homogeneous BSE in the present model [5], see Table II. It is seen from Fig. 9 that both forms of the resonant-improved BC Ansatz simulate the behavior of  $F_\pi(Q^2)$  produced by the vertex BSE solution quite well.

The obtained values of  $r_\pi$  are shown in Table I for the approximations discussed above. Also shown there is the charge radius produced by using the two dominant amplitudes  $F_1$  and  $F_5$  for the resonant addition to the BC Ansatz. Compared to  $r_{\pi,\text{BC}}^2 = 0.18 \text{ fm}^2$ , all versions of a resonant-improved BC Ansatz provide results roughly a factor of two higher and in significantly better agreement with the result from the vertex BSE solution and the experimental data. When the five dominant  $\rho$  amplitudes are used, the resonant-improved BC Ansatz reproduces the vertex BSE result for  $r_\pi$  to within 5%. The error increases to 10% if only the single dominant vector meson covariant is used for the resonant term of the vertex; part of the reason for this is due to the increase in the vector meson mass [5]: with  $F_1$  only,  $m_\rho^2 = 0.766 \text{ GeV}^2$ , which moves the pole 30% further into the timelike region.

Use of Eq. (32) allows  $r_\pi^2$  to be characterized as a resonant addition to the result of the BC Ansatz. If we write the difference between  $r_\pi^2$  and the BC contribution  $r_{\pi,\text{BC}}^2$  as

$$r_\pi^2 - r_{\pi,\text{BC}}^2 = \frac{6 g_{\rho\pi\pi} F_{V\pi\pi}(0)}{m_\rho^2 g_\rho}. \quad (33)$$

and compare this with Eq. (2), we see that  $F_{V\pi\pi}(0)$  characterizes the necessary weakening of the VMD mechanism for  $r_\pi^2$  to account for the distributed  $\bar{q}q$  substructure. The values of  $F_{V\pi\pi}(0)$  defined by Eq. (33), using the experimental values for  $g_{\rho\pi\pi}$ ,  $m_\rho$ , and  $g_\rho$ , are also shown in Table I. The difference between the  $r_\pi^2$  result from the vertex BSE solution and  $r_{\pi,\text{BC}}^2$  represents about 60% of the VMD value for the charge radius,  $r_{\pi,\text{VMD}}^2 = 0.48 \text{ fm}^2$ . The result from the best resonant-improved BC Ansatz (using the vector meson amplitudes  $F_1 - F_5$ ) shows that the resonant term is contributing to  $r_\pi^2$  at the level of 50% of the VMD value. This decreases somewhat when the description of the vector meson is simplified. One can attribute this weakening of the VMD mechanism at  $Q^2 = 0$  to the fact that the photon couples to a distributed, interacting  $\bar{q}q$  correlation and a significant part of this is already accounted for by the BC Ansatz for the vertex. With the remainder viewed as due to the  $\rho$  resonance, its effect is overestimated if, for example, the coupling to  $\pi\pi$  is described by the physical mass-shell value  $g_{\rho\pi\pi}$ . The effective reduction of the  $g_{\rho\pi\pi}$  is evidently about 50% in the present approach; this supports the previous cruder estimate [2].

In a more phenomenological approach, using parameterized quark propagators fitted to pion observables including  $r_\pi$  as was done in Ref. [7], one obtains a much better value for  $r_\pi$  using a BC Ansatz. In such an approach the  $Q^2$ -dependence of the vertex is parameterized

via the quark propagator, and can thus give a fair representation of the pion form factor. The charge radius obtained in this way,  $r_\pi = 0.55$  fm, is much closer to the experimental value than the one in the present work using a BC Ansatz. This is also an indication of the model-dependence and arbitrariness of separating the contributions into resonant and non-resonant terms.

The utility of the BC Ansatz for studies of electromagnetic coupling to hadrons is that it is completely specified in terms of the quark self-energy amplitudes. For similar reasons we seek to summarize the main features of the BSE solution for the quark-photon vertex also in terms of the quark self-energy amplitudes and a phenomenological  $\rho$ -meson BS amplitude, based on the resonance formula Eq. (30). For the  $\rho$  BS amplitude we use a simple Ansatz for the dominant amplitude only,  $F_1^V(q^2) \rightarrow N_\rho/(1 + q^4/\omega^4)$ , properly normalized and with  $\omega = 0.66$  GeV to give a decay constant  $f_\rho = 201$  MeV, similar to the parameterization used in Ref. [14]. In order to construct an Ansatz which can be used both at small and at large  $Q^2$ , we consider the following phenomenological form for  $Q^2 \geq -m_\rho^2$

$$\Gamma_\mu(q; Q) = \Gamma_\mu^{\text{BC}}(q; Q) - \gamma_\mu^T \frac{N_\rho}{1 + q^4/\omega^4} \frac{f_\rho Q^2}{m_\rho(Q^2 + m_\rho^2)} e^{-\alpha(Q^2 + m_\rho^2)}. \quad (34)$$

Since the correct UV asymptotic limit is provided by  $\Gamma_\mu^{\text{BC}}$ , the parameter  $\alpha > 0$  provides for a  $Q^2$  suppression of the resonant term. We fit  $\alpha$  to  $r_\pi$ , using the experimental values for  $m_\rho$  and  $f_\rho$ , and find good agreement with  $\alpha = 0.03$  GeV<sup>-2</sup>. The form factor  $F_\pi(Q^2)$  produced by this phenomenological vertex is shown in Fig. 9, and is seen to provide an excellent fit to the vertex BSE solution, and hence according to Fig. 7, also to the experimental data. Extensions to a more realistic  $\rho$  BS amplitude are straightforward to implement in phenomenological model calculations.

## V. SUMMARY AND OUTLOOK

We have used a ladder truncation for the BSE for the quark-photon vertex, in conjunction with a ladder-rainbow truncation for the quark DSE. Both the vector WTI for the quark-photon vertex and the axial-vector WTI are preserved in this truncation. This ensures both current conservation and the existence of massless pseudoscalar mesons if chiral symmetry is broken dynamically: pions are Goldstone bosons [4]. The details of the model were fixed in previous work [5]. It leads to dynamical chiral symmetry breaking and confinement; furthermore, at large momenta, our effective interaction reduces to the perturbative running coupling and thus preserves the one-loop renormalization group behavior of QCD and reproduces perturbative results in the ultraviolet region. The model gives a good description of the  $\pi$ ,  $\rho$ ,  $K$ ,  $K^*$  and  $\phi$  masses and decay constants [5].

Our numerical solution of the vertex BSE shows clearly the vector meson pole in all eight transverse amplitudes. At the photon momentum  $Q = 0$ , the solution agrees perfectly with the BC Ansatz, as required by the WTI and gauge invariance. Also at spacelike asymptotic momenta our transverse solution agrees with the BC Ansatz: both go to the bare vertex. At small but nonzero  $Q^2$  the BSE solution departs significantly from the BC Ansatz: the BSE solution has a stronger  $Q^2$ -dependence. In the region  $-m_\rho^2 < Q^2 < 0.2$  GeV<sup>2</sup>, the quark-photon vertex can be described by a BC Ansatz plus a resonant term. However, there

is no unique decomposition of the vertex into resonant and non-resonant terms away from the pole, and the BSE solution for the vertex is the appropriate representation containing both aspects.

Subsequently, we have calculated the pion charge form factor in impulse approximation. The results using the BSE solution for the  $\bar{q}q\gamma$  vertex are in excellent agreement with the data, see Fig. 7, and produce  $r_\pi^2 = 0.46 \text{ fm}^2$ , *without fine tuning the model parameters*: the parameters are completely fixed in Ref. [5]. Use of the BC Ansatz generally leads to a charge radius which is too low: in the present model, the resulting  $r_\pi^2 = 0.18 \text{ fm}^2$  is less than half the experimental value, while the remainder can be described by a  $\rho$  resonant term. This indicates that as much as half of  $r_\pi^2$  can be attributed to a reasonable extrapolation of the  $\rho$  resonance mechanism. On the other hand, the strict VMD picture is too simple; about half of  $r_\pi^2$  arises from the non-resonant photon coupling to the quark substructure of the pion. One should however keep in mind that such a separation in resonant and non-resonant contributions is ambiguous and model-dependent.

The form factor  $F_\pi(Q^2)$  exhibits a resonance peak at timelike momenta  $Q^2$  near  $-m_\rho^2$ , and our calculated  $F_\pi(Q^2)$  does indeed show such a peak. Since in ladder truncation one does not generate a width for the  $\rho$  meson, we overshoot the data close to the  $\rho$ -pole. We expect that if we include the  $\pi\pi$  mechanism for the  $\rho$  width in our formalism, we will have better agreement with the data in the timelike region. A detailed comparison close to the  $\rho$ -pole will be postponed until we have included this effect in our calculations.

Pion loops will not only generate a width for the  $\rho$ , they will also give a direct contribution to the pion form factor and generate a nonzero imaginary part for momenta  $Q^2 < -4m_\pi^2$ . Estimates are that the pion charge radius increases by 10% to 15% [15] due to pion loops, which would lead to a charge radius which is too large in the present model. However, the pion loops will also affect the calculated meson masses: estimates for the shift in the  $\rho$  mass vary between 2% and 10% [22], and the parameters in the effective quark-antiquark coupling will have to be readjusted to maintain agreement with the experimental data. We hope to address these question in future work.

With our BSE solution for the  $\bar{q}q\gamma$  vertex we can now investigate other hadron form factors. First results indicate [23] that also the  $\gamma^*\pi\gamma$  transition form factor at low  $Q^2$  is reasonably well described with the present vertex BSE solution. In the near future we will also apply this method to the kaon form factor and to electromagnetic decays such as  $\rho \rightarrow \pi\gamma$ . Another interesting application is the nucleon form factor, using models for the nucleon such as those being developed in Refs. [11,24]. The phenomenological resonance addition to the BC Ansatz, Eq. (34), can be used as guidance for phenomenological models to facilitate these and other hadron form factor calculations, without having to solve the vertex BSE numerically.

## ACKNOWLEDGMENTS

We acknowledge useful conversations and correspondence with C.D. Roberts, and D. Jarecke. This work was funded by the National Science Foundation under grant No. PHY97-22429, and benefited from the resources of the National Energy Research Scientific Computing Center.

## REFERENCES

- [1] H.B. O’Connell, B.C. Pearce, A.W. Thomas, and A.G. Williams, *Prog. Part. Nucl. Phys.* **39**, 201 (1997).
- [2] P.C. Tandy, in *Future Directions in Quark Nuclear Physics*, Eds. A.W. Thomas and A.G. Williams, (World Scientific, Singapore, 1999), p. 62-71.
- [3] M.R. Frank, *Phys. Rev. C* **51**, 987 (1995).
- [4] P. Maris and C.D. Roberts, *Phys. Rev. C* **56**, 3369 (1997).
- [5] P. Maris and P.C. Tandy, nucl-th/9905056, “Bethe–Salpeter studies of vector meson masses and decay constants” nucl-th/9905056, *Phys. Rev. C*, to be published, (1999).
- [6] C.D. Roberts, *Nucl. Phys.* **A605**, 475 (1996).
- [7] P. Maris and C.D. Roberts, *Phys. Rev. C* **58**, 3659 (1998).
- [8] C.J. Burden, C.D. Roberts and M.J. Thomson, *Phys. Lett. B* **371**, 163 (1996).
- [9] P.C. Tandy, *Prog. Part. Nucl. Phys.* **39**, 117 (1997).
- [10] F.T. Hawes and M.A. Pichowsky, *Phys. Rev. C* **59**, 1743 (1999).
- [11] J.C.R. Bloch, C.D. Roberts, S.M. Schmidt, A. Bender, and M.R. Frank, “Nucleon form factors and a nonpointlike diquark”, nucl-th/9907120, *Phys. Rev. C*, to be published (1999).
- [12] J.S. Ball and T.W. Chiu, *Phys. Rev. D* **22**, 2542 (1980).
- [13] D.C. Curtis and M.R. Pennington, *Phys. Rev. D* **42**, 4165 (1990).
- [14] M.A. Ivanov, Yu.L. Kalinovsky and C.D. Roberts, *Phys. Rev. D* **60**, 034018 (1999).
- [15] R. Alkofer, A. Bender, and C.D. Roberts, *Int. J. Mod. Phys.* **A10**, 3319 (1995).
- [16] P. Maris, C.D. Roberts and P.C. Tandy, *Phys. Lett. B* **420**, 267 (1998).
- [17] V.A. Miransky, *Phys. Lett. B* **165**, 401 (1985); D. Atkinson and P.W. Johnson, *Phys. Rev. D* **37**, 2296 (1988).
- [18] F.T. Hawes, P. Maris, and C.D. Roberts, *Phys. Lett. B* **440**, 353 (1998).
- [19] C.J. Bebek *et al.*, *Phys. Rev. D* **13**, 25(1976).
- [20] L.M. Barkov *et al.*, *Nucl. Phys.* **B256**, 365 (1985).
- [21] S.R. Amendolia *et al.*, *Nucl. Phys.* **B277**, 168 (1986).
- [22] L.C.L. Hollenberg, C.D. Roberts and B.H.J. McKellar, *Phys. Rev. C* **46**, 2057 (1992); D.B. Leinweber and T.D. Cohen, *Phys. Rev. D* **49**, 3512 (1994); K.L. Mitchell and P.C. Tandy, *Phys. Rev. C* **55**, 1477 (1997); M.A. Pichowsky, S. Walawalkar, and S. Capstick, “Meson-loop contributions to the rho-omega mass splitting and rho charge radius”, nucl-th/9904079.
- [23] P. Maris and P.C. Tandy, “The quark-photon vertex and meson electromagnetic form factors”, nucl-th/9908045, to appear in the proceedings of PANIC’99, June 1999, Uppsala University, Eds. S. Kullander, G. Fäldt, and B. Höistad.
- [24] R. Alkofer, S. Ahlig, C. Fishcer, M. Oettel, and H. Reinhardt, “Octet and decuplet baryons in a confining and covariant diquark-quark model”, hep-ph/9907563, to appear in the proceedings of PANIC’99, June 1999, Uppsala University, Eds. S. Kullander, G. Fäldt, and B. Höistad.

# FIGURES

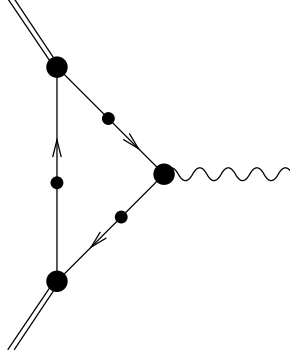


FIG. 1. The impulse approximation for the pion charge form factor.

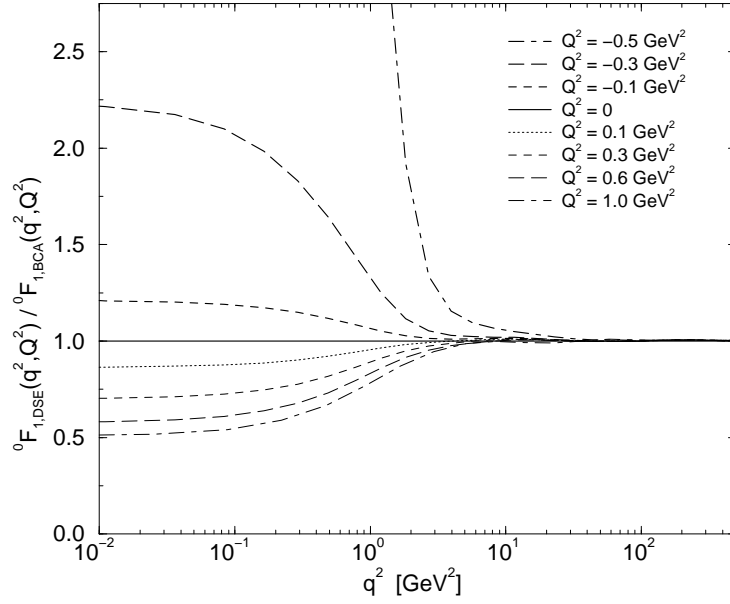


FIG. 2. The ratio of the BSE solution over the BC Ansatz for the dominant amplitude  ${}^0F_1$ , associated with  $\gamma_\mu^T$ , of the quark-photon vertex as function of  $q^2$  for the indicated values of the photon momentum  $Q^2$ . The quark momenta are  $q \pm Q/2$ .



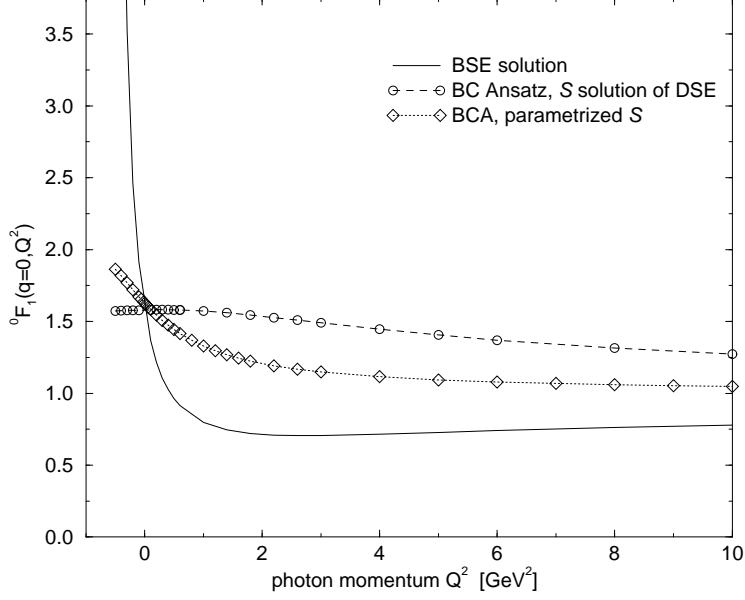


FIG. 3. The  $Q^2$ -dependence of the BSE solution for the dominant amplitude  ${}^0F_1$  of the  $\bar{q}q\gamma$  vertex at  $q^2 = 0$  (solid line). The dashed line with circles is the BC Ansatz for this amplitude in the present model; the dotted line with diamonds is the BC Ansatz with phenomenological quark propagator functions  $A$  and  $B$  parameterized and fitted to pion observables, including  $r_\pi$ , according to Ref. [7].

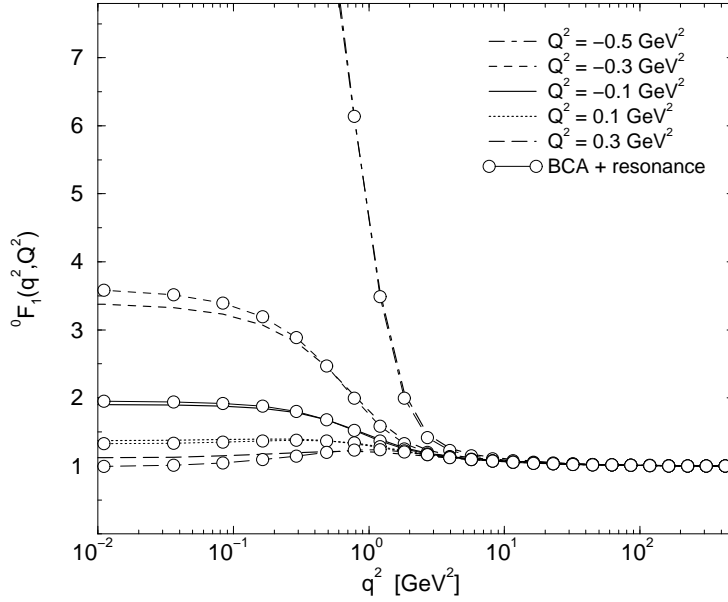


FIG. 4. The  $q^2$ -dependence of the BSE solution for the dominant amplitude  ${}^0F_1$  for a range of timelike and spacelike values of the photon momentum  $Q^2$ . The circles correspond to the resonant-improved BC Ansatz as described in the text.

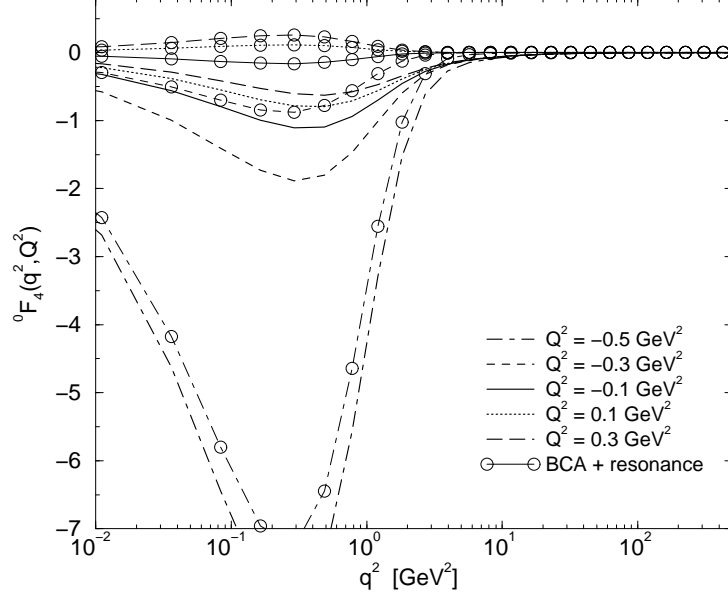


FIG. 5. The same as Fig. 4 except now for the  $\bar{q}q\gamma$  vertex amplitude  ${}^0F_4$ .

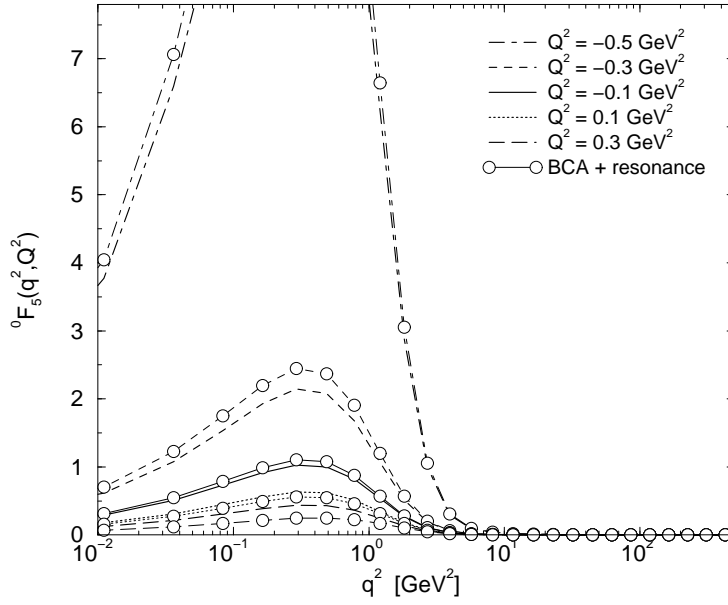


FIG. 6. The same as Fig. 4 except now for the  $\bar{q}q\gamma$  vertex amplitude  ${}^0F_5$ .

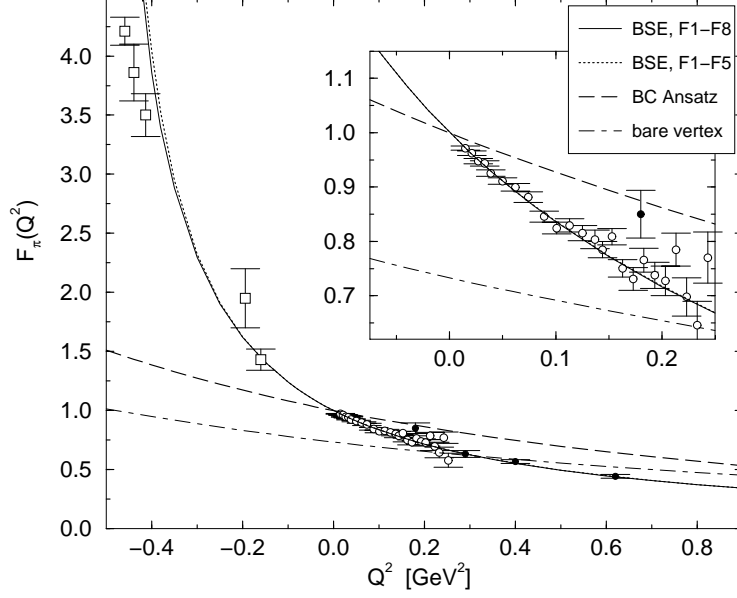


FIG. 7. The pion charge form factor  $F_\pi(Q^2)$  as obtained from different treatments of the quark-photon vertex. The inset shows the  $Q^2$  region relevant for the charge radius. The data correspond to  $|F_\pi|$ , taken from Refs. [19] (circles), [20] (squares), and [21] (dots).

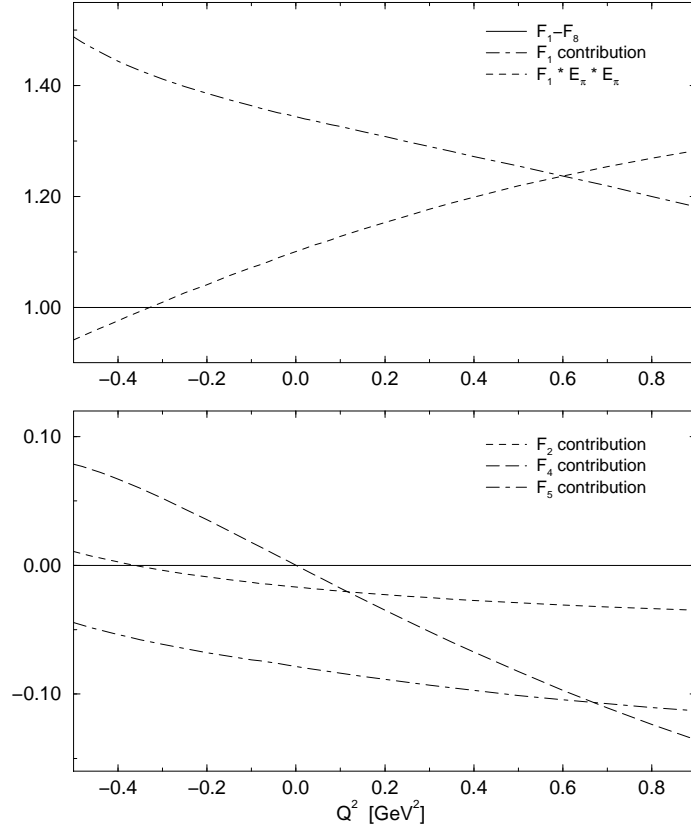


FIG. 8. The relative contributions to  $F_\pi(Q^2)$  from the four most important amplitudes  $F_1$  (top),  $F_2$ ,  $F_4$ , and  $F_5$  (bottom) of the BSE solution for the  $\bar{q}q\gamma$  vertex. For the dominant amplitude  $F_1$ , we also display the relative contribution from the dominant pion amplitudes  $E_\pi$  only (top).

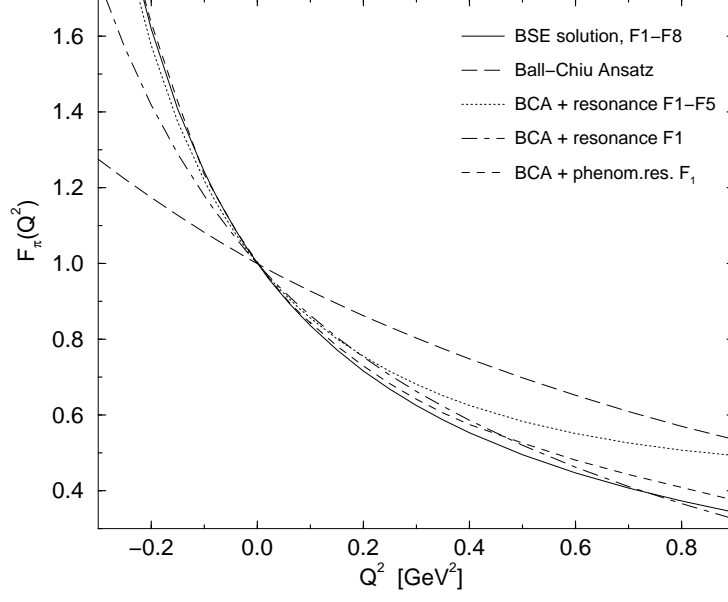


FIG. 9. The pion charge form factor  $F_\pi(Q^2)$  as obtained from different descriptions of the quark-photon vertex in terms of a resonant-improved BC Ansatz, and compared to  $F_\pi(Q^2)$  as obtained from the vertex BSE solution.

TABLES

photon vertex	$r_\pi$	$r_\pi^2$	$r_\pi^2 - r_{\pi,BC}^2$	$F_{V\pi\pi}(0)$
Expt. [21]	$0.663 \pm 0.0006$	$0.44 \pm 0.0012$		
DSE $F_1 - F_8$	0.678	0.460	0.278	0.58
DSE $F_1 - F_5$	0.677	0.459	0.277	0.58
BC Ansatz (BCA)	0.426	0.182		
BCA + res. $F_1 - F_5$	0.640	0.409	0.227	0.47
BCA + res. ( $F_1$ & $F_5$ )	0.625	0.390	0.208	0.44
BCA + res. $F_1$	0.605	0.366	0.184	0.38
BCA + phenom.res. $F_1$	0.68	0.46	0.28	0.58
BCA of Ref. [7]	0.55	0.30		

TABLE I. Results for the pion charge radius according to various treatments of the quark-photon vertex.  $F_{V\pi\pi}(0)$  roughly characterizes the reduction in the  $\pi\pi$  coupling strength for the vector  $\bar{q}q$  correlation in the vector vertex compared to the on-shell coupling to the  $\rho$ ,  $g_{\rho\pi\pi}$ .

	$m_\rho$	$f_\rho$
Expt.	0.770	0.216
$F_1 - F_8$	0.742	0.207
$F_1 - F_5$	0.730	0.201
$F_1$ & $F_5$	0.765	0.203
$F_1$	0.875	0.20

TABLE II. The vector meson mass  $m_\rho$  and decay constant  $f_\rho$  in GeV corresponding to various truncations of the eight possible invariant amplitudes of the  $\rho$  BS amplitude [5].